NJC

Accepted Manuscript

This is an *Accepted Manuscript*, which has been through the Royal Society of Chemistry peer review process and has been accepted for publication.

Accepted Manuscripts are published online shortly after acceptance, before technical editing, formatting and proof reading. Using this free service, authors can make their results available to the community, in citable form, before we publish the edited article. We will replace this *Accepted Manuscript* with the edited and formatted *Advance Article* as soon as it is available.

You can find more information about *Accepted Manuscripts* in the Information for Authors.

Please note that technical editing may introduce minor changes to the text and/or graphics, which may alter content. The journal's standard Terms & Conditions and the Ethical guidelines still apply. In no event shall the Royal Society of Chemistry be held responsible for any errors or omissions in this *Accepted Manuscript* or any consequences arising from the use of any information it contains.

ROYAL SOCIETY OF CHEMISTRY

www.rsc.org/njc

Eco-friendly synthesis of bimetallic AuAg nanoparticles

Amanda G. Garcia[1,*], Pietro P. Lopes[1], Janaina F. Gomes[1], Cleiton Pires[1], Eduardo B. Ferreira[1], Rubens G. M. Lucena[2], Luiz H. S. Gasparotto[1,2†] and Germano Tremiliosi-Filho[1]

[1]*Instituto de Química de São Carlos, Universidade de São Paulo, Caixa Postal 780, 13560-970 São Carlos, SP, Brazil*

[2]*Instituto de Química, Universidade Federal do Rio Grande do Norte, Lagoa Nova, 59072-970, Natal, RN, Brazil*

**Corresponding author:* Ph.D. Amanda Cristina Garcia

E-mail: amandagarcia@iqsc.usp.br

phone: +55 16 3373 9934 fax: +55 16 3373 9903

Keywords: glycerol oxidation, nanoparticle synthesis method, AuAg bimetallic nanoparticle, alkaline medium, direct glycerol fuel cell.

† Current address

Abstract

In this study we report a friendly route to produce colloidal AuAg bimetallic nanoparticles (NPs) using glycerol as reducing chemical in alkaline medium. Ultraviolet spectroscopy (UV-Vis) and transmission electron microscopy (TEM) confirmed the formation of colloidal NPs. The nanoparticles were also directly produced onto carbon to yield Au/C, Ag/C and AuAg/C. Extended X-ray absorption fine-structure (EXAFS) spectroscopy at the Au L_3 edge evidenced surface segregation of silver in the AuAg/C material. Also the X-ray absorption near edge structure (XANES) region indicated a slight reduction in the Au 5*d* band occupancy due the presence of silver. Since Fuel Cell is a potent source of energy for the future, the catalytic properties of the NPs were then investigated for anodic glycerol electro-oxidation reaction and results for AuAg NPs are compared with those for monometallic Au and Ag NPs. When compared with Au/C, the AuAg/C material displayed lower potential for glycerol electro-oxidation, reducing by 120 mV the onset potential for glycerol electro-oxidation. This means that the electro-oxidation of glycerol at the bimetallic catalyst is mainly affected by the ligand effect.

1. Introduction

The physical and chemical properties of nanostructured metallic materials are very different from their corresponding bulk counterpart. For example, the availability of a large number of reactive sites in a curved surface of a nanoparticle favors the adsorption of chemicals, which improves the chemical reactivity of the material. Aspect of this type has catapulted the development, characterization and application of metallic nanoparticles in heterogeneous catalysis, ultrafast data communication and optical data storage[1,2,3]. Silver and gold have been thoroughly studied because of their broad absorption band in the visible region of the electromagnetic spectrum. Colloidal solutions of these metals are very intensely colored, which is absent in the bulk materials. This characteristic is interesting for surface-enhanced Raman spectroscopy[4], for example, that makes use of the local-enhanced electric field for detection of molecules at very low concentrations.

A variety of methods of synthesis, such as polyol[5] and microwave assisted[6], may be employed in the production of Au and Ag Nps, for example. The polyol method typically consists in refluxing a mixture of a precursor salt (e.g., $AuCl_3$ or $AgNO_3$), a stabilizing agent [e.g., poly (vinyl pyrrolidone) (PVP)] and a polyalcohol (e.g., ethylene glycol) at ~160–240 °C for 2–12 h, which requires a long time and energy consuming. The microwave-assisted approach also requires high temperature and has the further inconvenience of demanding a microwave generator.

In this study a facile green route based on co-reduction of Au^{3+} and Ag^{+} by glycerol in alkaline medium at room temperature was used to synthesize bimetallic colloidal nanoparticles as well as AuAg-NPs anchored onto a carbon support. Carbon-supported AuAg nanoparticles were then tested for glycerol electrooxidation. The

AuAg colloidal nanoparticles were analyzed by ultraviolet-visible spectroscopy (UV-Vis) and transmission electron microscopy (TEM). Energy-dispersive X-ray (EDX) spectroscopy, X-ray diffraction (XRD) and TEM were employed to characterize the AuAg anchored on carbon. Changes in the electronic and structural properties of Au, induced by the presence of Ag, were probed by *in situ* X-ray absorption near edge structure (XANES) and extended X-ray absorption fine-structure (EXAFS) spectroscopies at the Au L_3 edge. EXAFS results indicated a more vacant gold 5*d* states in the AuAg material than in the pure Au, an effect more pronounced with increasing electrode potential. This electronic effect was correlated with the decrease of 120 mV in the onset potential for glycerol electro-oxidation. Although the electrooxidation of glycerol started at a lower potential compared to that of pure gold, the current magnitude also decreased, a consequence of lower availability of gold sites. Catalysis enhancement is generally explained in terms of the bifunctional mechanism[7] and ligand effect[8], with both effects being normally inseparable. Herein we present tangible evidence that the ligand effect plays the definitive role in the reaction, whereas the bifunctional mechanism is unimportant.

2. Experimental Section

2.1 Synthesis of Colloidal and Carbon-Supported $Au_{50}Ag_{50}$-NPs

For the production of bimetallic colloidal nanoparticles, the following stock solutions were produced: 40 g L^{-1} polyvinylpyrrolidone (PVP) (MW = 10,000), 10 mmol L^{-1} $AuCl_3$ (30% wt in HCl), 10 mmol L^{-1} $AgNO_3$ and 1.0 mol L^{-1} glycerol + 0.10 mol L^{-1} NaOH. In a beaker, 50 μL of the $AuCl_3$ solution, 50 μL of the $AgNO_3$ solution and 2.5 mL of the PVP solutions were mixed and water was further added to

yield a 5.0-mL solution. In a separate vessel, 1.0 mL of the glycerol-NaOH solution was dissolved in ultrapure water to yield a 5.0-mL solution. The glycerol-NaOH solution was then added to the $AuCl_3$-$AgNO_3$-PVP solution to generate a 10-mL solution with the following final concentrations: 0.050 mmol L^{-1} Au^{3+}, 0.050 mmol L^{-1} Ag^{+}, 0.10 mol L^{-1} glycerol, 0.010 mol L^{-1} NaOH and 10 g L^{-1} PVP.

Gold[9]**Error! Bookmark not defined.** and silver[10] monometallic NPs were also synthesized to compare the results with those of AuAg-NPs. For the preparation of monometallic NPs, the procedure was similar, however the concentrations of Au^{3+} and Ag^{+} were 0.10 mmol L^{-1} for both, whereas the concentrations of glycerol, NaOH and PVP remained the same.

For the electrocatalytic experiments, all nanoparticles were synthesized using the same procedure applied for the synthesis of colloidal nanoparticles. However, the nanoparticles were produced directly onto Vulcan carbon (NPs/C) without stabilization by PVP, thus avoiding any influence of PVP on the reactions under study. The synthesis of the bimetallic catalyst consisted in sonicating 40 mg of XC-72 Vulcan carbon in 50 mL of ultrapure water and then adding a fixed amount of $AuCl_3$ and $AgNO_3$ under stirring to promote homogenization. Afterwards, another aqueous solution containing glycerol and NaOH was added to give the following concentrations: 0.20 mmol L^{-1} Au^{3+}, 0.20 mmol L^{-1} Ag^{+}, 1.0 mol L^{-1} glycerol and 0.010 mol L^{-1} NaOH. The black suspensions were kept during 24 h under stirring at room temperature and then washed, filtered and dried at 80 °C for 12 h. To produce Au/C and Ag/C monometallic catalysts the method employed also was similar, although for this materials the concentration were 0.40 mmol L^{-1} Au^{3+} and 0.40 mol L^{-1} Ag^{+}.

2.2 Characterization of the nanomaterials

In order to analyze the efficiency of the synthesis method employed, the colloidal suspensions were characterized with UV-Vis and TEM. UV-Vis spectra of the colloidal NPs suspensions were acquired with a Varian/Cary 5G spectrophotometer. For TEM analyses, carbon-coated copper grids were immersed into AuNPs, AgNPs and AuAgNPs colloidal suspensions and allowed to dry in a desiccator overnight. The grids were then analyzed using a TEM FEI Tecnai with an accelerating potential of 200 kV. The NPs/C were also evaluated by TEM FEI Tecnai. For NPs/C the copper-coated grids were dipped in a suspension containing 1.0 mg of catalytic powder and 5 mL of isopropanol alcohol.

EDX was employed to determine the molar ratio of metal/carbon (wt %) of the nanoparticles dispersed onto carbon. XRD was also used to observe the diffraction pattern and to estimate the average crystallite size from the Scherrer's equation[11]:

$$D = k\lambda / \mathrm{B}\cos\theta \qquad (1)$$

where D is the average crystallite size in angstrom, k is a coefficient taken here as 0.9, λ is the wavelength of the X-rays used (1.5406 Å), B is the full width at half maximum of the diffraction peak, given in radians, and θ is the angle at the position of the peak maximum, given in degrees.

To investigate the structure of the bimetallic nanoparticles and to understand the effect caused by the presence of silver, the electronic properties of the material were investigated with *in situ* X-ray absorption spectroscopy (XAS) in the XANES and EXAFS regions at the Au L_3 absorption edge (11919 keV). The working electrodes employed for the measurements consisted of appropriated amount of catalysts (Au metal load of 6 mg cm^{-2}) bound with Nafion (5 wt.%) suspended in isopropyl alcohol and carried to ultrasonic homogenization, after the solvent was

evaporated at room temperature. The catalyst powder was then deposited on a disc of carbon cloth (geometric area = 0.95 cm^2) and pressed at room temperature.

These measurements were conducted at 0.5 V and 0.95 V *vs.* RHE in 0.1 mol L^{-1} NaOH. All XAS experiments were carried out at the D04B-XAFS1 beam line in the National Synchrotron Light Source Laboratory (LNLS), situated in Campinas, Brazil. X-ray absorption spectra were collected in transmission mode with three ionization chambers (incidence I_0, transmitted I_t, and reference I_r). The reference channel was used mainly to calibrate the edge position with a pure Au foil sample. The IFEFFIT software package was used to analyze the XAS data. Further details can be found in the literature[12].

2.3 Electrochemical Measurements

The electrochemical experiments were conducted in a conventional three-electrode cell. A catalytic layer of NPs/C on a glassy carbon disc, a gold foil and a reversible hydrogen electrode in 0.1 mol L^{-1} NaOH were employed as working, counter and reference electrodes, respectively. A glassy carbon disc (ϕ_{OD} = 5 mm, geometric area = 0.196 cm^2) was used as substrate to support active layers of NPs/C. For the preparation of the catalytic layer, 2.0 mg of the catalytic powder (Au/C, Ag/C or AuAg/C) were suspended in a mixture containing 1 mL of isopropyl alcohol and 20 μL of a Nafion solution (5 wt % in low aliphatic alcohol, from DuPont). After ultrasonic homogenization, 20 μL of this ink were deposited onto the glassy carbon disc and the solvent was then evaporated at room temperature. Electrochemical measurements were performed in 0.1 mol L^{-1} NaOH + 0.1 mol L^{-1} glycerol solutions prepared with ultrapure water.

The electrochemical experiments were conducted with a computer-controlled potentiostat (AutoLab PGSTAT 30). Cyclic voltammetry (CV) was carried out in the range of 0.01 to 1.6 V vs. RHE after deoxygenating the solution with argon. All experiments were performed at $v = 50$ mV s^{-1}.

3. Results and Discussion

3.1. Physical and chemical properties of the nanomaterials

A first way to confirm the effectiveness of the synthesis method to produce nanometric sized materials was the production of unsupported Au, Ag and AuAg-NPs. UV-Vis spectra of the colloidal Au, Ag and AuAg-Nps prepared at room temperature (~25 ^{o}C) using glycerol in alkaline medium as reducing agent are displayed in Fig. 1A. The spectrum of colloidal AuNps presented a maximum absorbance at around 520 nm, a wavelength corresponding to quasispherical gold nanoparticles[13,14]. After reduction of the Au^{3+} to Au^{0} the solution turned to a deep-red color, reflecting the surface plasmon band (SPB) characteristic for gold in the nanometric regime. The colloidal AgNps presented a maximum absorbance at around 410 nm, a value that is attributed to the silver SPB. Fig. 1A also presents UV-Vis spectra of bimetallic AuAgNPs with molar ratio of 1:1. Alloy formation of bimetallic nanoparticles is evidenced by the appearance of a single band which λ_{max} is located between those of pure Au and Ag nanoparticles according to literature data[15,16]. This is the first evidence of the capability of glycerol employed as reducing agent in generating gold, silver and gold/silver nanoparticles.

Correspondent TEM images of colloidal NPs are also showed in Fig. 1B. For Au-NPs most of nanoparticles were spherical in shape, thus corroborating the UV-Vis

spectra, whereas Ag and AuAgNPs are larger than AuNPs and tended to agglomerate. According to TEM images, the average sizes of the Au, Ag and $Au_{50}Ag_{50}$-NPs were 10.0, 20.0 and 15 nm, respectively.

A point worth mentioning is the absence of hollow $Au_{50}Ag_{50}$-NPs particles, which implies that galvanic replacement of silver ions by gold ones did not take place. It is well known that if silver nanoparticles are firstly produced with posterior addition of $HAuCl_4$, hollow structures with walls made of Au-Ag alloys are formed[17,18,19]. The nanoparticles also undergo reconstruction with the formation of porous walls via dealloying, which impacts their shape causing a gradual redshift and peak broadening in the spectra as the Au^{3+} concentration increases. Fig 2A shows the effect of adding $HAuCl_4$ to previously formed AgNPs. One can see that the increase of the Au^{3+} concentration led to a gradual absorbance decrease, redshift, and peak broadening, a behavior consistent with etched and porous-walled nanoparticles[17,18,19]. However, by reducing simultaneously Au^{3+} and Ag^{+} we preserved the spherical shape of the nanoparticles in this work, thus eliminating a possible effect of the nanoparticle shape on the electrocatalysis. Another question is the deposition of silver on previously formed gold nanoparticles. Fig 2B shows UV-vis spectra of AgAu nanoparticles produced by adding $AgNO_3$ into a solution containing gold nanoparticles. Unlike silver nanoparticles gold does not suffer etching and the gradual blueshift in the UV-vis suggests that silver layers were deposited onto gold nanoparticles[20]. Furthermore, in contrast to the UV-vis features of the silver nanoparticles, the peak broadening decreased with Ag^{+} concentration, thus suggesting preservation of the original spherical structure.

As the synthesis method is shown to be effective to produce nanometric sized Au, Ag and AuAg nanomaterials, we also employed the reduction route to obtain the same set of materials directly supported onto carbon, however without PVP. Although

one can anchor PVP-stabilized colloidal NPs onto carbon (NPs/C), the presence of PVP might alter the electrochemical activity. As the route of PVP removal is not straightforward, we synthesized the same set of materials directly onto carbon with the same reduction procedure but without the addition of PVP. One can observe that although a surfactant as PVP is absent in the synthesis of the supported nanoparticles, the nanoparticles were kept in the nanoregime, what suggests that the carbon support played a role in preventing excessive growth of the nanoparticles.

Fig. 3A shows the XRD pattern corresponding to the Au, Ag and AuAg nanoparticles anchored onto Vulcan carbon. The XRD pattern revealed the typical face-centered cubic (fcc) structure of silver and gold[21] and was further analyzed using the Scherrer's equation[11] in order to estimate the average crystallite size. For the AuAg/C all reflections are similar to monometallic Au and Ag since both metals have very similar lattice constants (Table 1). Therefore, no shift of reflections for the AuAg NPs was observed, as it would be expected for alloyed materials. Considering the 220 crystallographic planes, the estimated mean crystallite size for the Au/C, Ag/C, and AuAg/C nanoparticles was 17, 19 and 14 nm, respectively.

TEM images were carried out to investigate the structure, shape, size, composition and dispersion of metal Au, Ag and AuAg nanoparticles dispersed on Vulcan carbon, the images are displayed in Fig. 3B. For AuNPs/C, the TEM image shows that nanoparticles are spherically shaped distributed over the carbon substrate. This result shows that, although the synthesis was performed in the absence of PVP (Section 2.1), gold can still be formed in a homogeneous spherical shape. The same was observed for Ag/C regarding their spherical-like shape, but in a rather nonhomogenous dispersion over the carbon substrate. Finally, in the AuAg/C TEM image it is possible to observe that the particles are in the form of nanocrystalline agglomerates distributed on the carbon substrate. One can identify gold, silver and

gold-silver alloy nanoparticles of 9 nm, 16 nm and 17 nm in size, respectively. The TEM pictures reveal a clear bimodal size distribution, which might be due to ripening and, hence, formation of extra small particles. Dissolution of small particles and redeposition on the surface of larger ones is possible due to the lack of PVP protection EDX analysis showed that the amounts of metal are near to the nominal values (10 wt. %), which were around 6.0 wt. % of metal dispersed on the carbon, for all synthesized materials. For bimetallic nanoparticles, EDX also showed a 1:1 Au:Ag bulk atomic ratio.

3.2. XAS results

3.2.1 EXAFS results

In order to analyze the local structure of the catalysts obtained from a simple green route, we used *in situ* XAS measurements in the EXAFS region employing a simple first-shell analysis that considers only Au-Au and Au-Ag coordination spheres, as the inclusion of any Au-O shell did not result in a better fitting of the EXAFS signal. We used a gold foil as reference to determine the theoretical-to-experimental correlation value S_0^2 used in the NPs data fitting. Fig. 4 shows a typical experimental data and their respective fitting for both AuNPs and AuAg-NPs, as well as for the gold foil. The fitting results (shown in Table 2) reveal that the Au/C has similar structural parameters than those for gold foil, in agreement with the XRD analysis (Table 1). On the other hand, examining the results for the AuAg/C material, one can identify a significant difference in the coordination numbers for both Au-Au and Au-Ag shells. As one can see from Table 2, the coordination number for Au-Ag pairs indicates a severe depletion of this type of bond pair in this nanoparticle, while Au-Au pairs are nearly similar to the Au/C material as well as the gold foil. Considering that

the EDX analysis shows an atomic composition close to 1:1 (Au:Ag), the reduced coordination number for Au-Ag shell indicates a segregation of silver, although based solely in these results it is not possible to determine the type of segregation. Moreover, regardless the electrode potential or the presence of glycerol, the average Au-Au distance for the AuAg-NPs/C is very close to that of gold metal, indicating that the presence of Ag in the material does not incur in significant change in the Au-Au coordination shell. This is consistent with the occurrence of silver in a segregated form, indistinctively if in ad-islands or shell-like structures. Segregation of silver at AuAg catalysts has been recently observed by Déronzier *et. al*[22] in the catalytic oxidation of carbon monoxide.

It is possible, however, to infer that silver is at the surface of the AuAg/C once the increase in the electrode potential raises the Au-Au coordination number, with or without glycerol in the solution. As oxygenated species are formed at the material surfaces at higher electrode potentials, these oxi/hydroxi species may be triggering a surface segregation of silver in a similar way to what was observed for PtRu materials [23] . Our findings are also in agreement with what was proposed by Christoffersen et al.[24]. Although their calculations suggest that gold-silver systems do not have a tendency to phase segregation, the presence of a third species, such as water or surface hydroxide, may pull the material with higher adsorption energy to the surface. In such way, as silver has more favorable interaction energy to form oxygenated species than gold, this would explain why we observe a tendency to silver surface segregation at higher electrode potentials. Also the Au-Ag bond distance is somewhat shorter than that observed for Au-Au bond at lower potentials, whereas the increase in the electrode potential expands this bond, consistent with the segregation effect discussed. When examining Au-Au coordination shell disorder parameter, one can observe that the values obtained for Au/C and AuAg/C are very close to the one

shown for the gold foil. Nonetheless, the change in electrode potential increases its value for the AuAg/C material, in agreement to a more disturbed Au-Au bond pairs due the silver segregation process.

We should mention other two aspects that could contribute for a richer silver surface. The first one is the formation of AgCl precipitate. The AgCl would, in turn, release Ag^+ slowly contributing for a surface richer in silver. Although we did not observe (by naked eye) turbidity upon mixing the $AgNO_3$ and $AuCl_3$ solutions, the formation of some AgCl is possible due to its low *K*ps (1.8×10^{-10}). The question is whether glycerol is able to generate AgNPs from AgCl. Fig. 5A shows a UV-vis spectrum of AgNPs produced from AgCl. For this we produced the AgCl precipitate by mixing 0.1 mol L^{-1} KCl with 0.1 mol L^{-1} $AgNO_3$, centrifuged it, removed the supernatant, re-dispersed the AgCl, and finally added alkalinized glycerol. The solution slowly turned yellow with an absorbance maximum around 410 nm, thus confirming that glycerol in alkaline medium is capable of generating AgNPs from the slow dissociation of AgCl in Ag^+ and Cl^-. The second aspect is the completely different kinetics of Au^{3+} and Ag^+ reduction by glycerol. Fig. 5B presents the evolution of absorbance for monometallic AuNPs and AgNPs at their respective λ_{max}. In both cases the concentration of metallic ions was 0.1 mmol L^{-1}. One notices that AuNPs are steadily formed from the beginning of the experiment, while the formation of AgNPs passes through an inducing period followed by an exponential increase in the reaction velocity. Therefore, according to Fig. 5B, it is possible to note that the formation mechanism of bimetallic nanoparticles occurs by two parallel pathways. In the beginning of the reaction, gold is quickly reduced while there is an induction time for the formation of metallic silver. This behavior suggests that in the case of AuAg-NPs formation, gold nuclei would be firstly formed with subsequent silver incorporation, thus explaining the richer silver surface. Similar mechanism was

observed for Fe-Rh (Chem. Mater., 19 (2007) 4624) and Ru-Cu (P. Arquilliere et al., Topics Catal, 56 (20113) 1192-1198) nanoparticles.

3.2.2 XANES results

To verify the electronic effect of silver addition on the gold electronic properties, *in situ* XANES spectra were recorded at the Au L_3 edge from samples at 0.5 V and 0.95 V, with results presented in Fig. 6. Gold has almost zero "white-line" due to filled $5d_{3/2}$ Au states. The first peak intensity points out for an almost zero effect of the electrode potential on pure AuNps, with only a slight tendency for increased vacancy at 0.95 V. This agrees with previous results on Pt electrodes[25], where formation of oxide layer would increase the L_3 "white-line" intensity indicating reduced electron occupancy in those states. On the other hand, the AuAg-NPs presented more pronounced shift in the "white-line" intensity, showing more vacant gold 5*d* states than the respective gold foil. The change of potential affects in a similar way the reduced electron occupancy, whereas the presence of glycerol does not seem to change the 5*d* band states as much as the potential or the presence of silver.

In summary, the EXAFS results evidence surface segregation of silver in the AuAg/C NPs, also present in the raw material and enhanced by the presence of surface oxygenated species at higher electrode potentials. In addition, the XANES region indicates a slight tendency of reduction in the Au 5*d* band occupancy due to (1) the presence of silver and (2) the increasing of the electrode potential, being effect (1) much less pronounced than effect (2).

3.3. Application of NPs/C - Glycerol electro-oxidation

In this section, results of glycerol electro-oxidation over AuAg/C are presented in Fig. 7. For comparison results for Au/C and Ag/C are also shown. For all materials one of the main activity features can be drawn from the onset potential, determined for all CV profiles as the potential where the oxidation current was slightly higher than the corresponding double-layer charging current. Therefore, in the positive-going potential scan, the onset potential of the glycerol electro-oxidation in alkaline medium for AuAg/C electrocatalyst is around 0.72 V *vs*. RHE and the peak current occurs at 1.32 V *vs*. RHE (Fig. 7a). The current then falls at higher potentials as a consequence of oxide formation, deactivating the gold surface. In the negative-going potential scan, the reactivation of the electrode appears at 1.4 V due to reduction of the gold oxides formed in the positive-going scan, which releases gold sites for reacting with glycerol molecules close to the surface.

The CV for Ag/C electrocatalyst is shown in Fig. 7b. In the potential range between 0.05 V and 1.6 V *vs.* RHE, the CV presents well-defined peaks characteristic of Ag in both presence and absence of glycerol[26]. In alkaline medium, the small peak at 1.2 V is attributed to the formation of a few monolayers of AgOH and Ag^+ species[23]. Peaks at around 1.3 and 1.6 V were assigned to the formation of inner hydrous oxide layer and more compact outer oxide layer, respectively. In the back scan, the reduction current peak at 1.3 and 1.0 V was ascribed to the electro-reduction of the silver oxides formed during the positive-going potential scan[23]. Similar profile was obtained for Ag/C electrocatalyst in presence of glycerol. Cyclic voltammogram shows that no glycerol electro-oxidation occurred at lower potential than Au/C. Noticeably, in the presence of 0.1 M glycerol the redox peaks of silver oxides were significantly shifted to higher potential, whilst no reactivation current of glycerol electro-oxidation was clearly evidenced for this electrocatalyst. This result implies that Ag/C is a very poor electrocatalyst to promote the glycerol electro-oxidation.

The catalytic activity of $Au_{50}Ag_{50}$/C electrocatalyst is different from those observed for the monometallic catalysts, as seen in Fig. 7c. A synergistic effect improved the catalytic performance of the $Au_{50}Ag_{50}$/C electrocatalyst. Particularly, the onset potential for glycerol electro-oxidation is around 0.6 V, representing a reduction of 120 mV compared to pure Au/C electrocatalyst. If one examines the first oxidation peak, the maximum current for $Au_{50}Ag_{50}$/C was about 0.56 mA, nearly ten times lower than that observed for Au/C, and the oxidation peak occurs at 1.2 V. With increasing electrode potential, the current then falls and at 1.4 V the current rises again, yielding a second peak that occurs at 1.45 V. This second peak is probably a contribution from the silver oxide peak, as observed for pure Ag/C electrocatalyst (Fig. 7b). In the negative-going potential scan, the reactivation of the electrode appears at 1.15 V, which can also be ascribed to the reduction of the gold oxides formed in the positive-going.

According to these results, electro-oxidation of glycerol at the bimetallic $Au_{50}Ag_{50}$/C electrocatalyst is mostly affected by the ligand effect. This means that the presence of silver would alter the electronic properties of gold causing glycerol to adsorb less strongly on gold. The XANES region indicated a slight tendency of reduction in the Au 5*d* band occupancy due to the presence of silver. As the rate of reaction is then dictated by the amount of available gold, it is natural that the current magnitude observed for the bimetallic catalyst is lower that that for pure gold. EXAFS results showed that silver is segregated to the surface of the nanoparticles, thus composing the majority of the surface area. Nevertheless, the gold in the surface of the AuAg electrocatalyst is more efficient in oxidizing glycerol, since glycerol oxidizes at about 120 mV earlier than Au/C. As already discussed, the AuAg/C electrocatalyst presents more vacant gold 5*d* states than the Au/C electrocatalyst, which is more pronounced with increasing electrode potential. This

electronic effect promoted by the Ag atoms reduces the Au density of states close to the Fermi level, which might tune the adsorption strength of adsorbates on the Au surface. Therefore, the presence of Ag in the Au structure provided an overall more efficient catalyst for glycerol oxidation in terms of the energy efficiency.

4. Conclusion

Colloidal and carbon-supported bimetallic $Au_{50}Ag_{50}$-NPs were easily synthesized using glycerol as reducing chemical in alkaline conditions. The maximum in the UV-Vis spectrum suggested the nanosized nature of the AuAg bimetallic NPs as well as Au and Ag monometallic nanoparticles, which was confirmed by TEM images. EXAFS results evidenced surface segregation of silver in the AuAg/C NPs, which is further promoted due the presence of surface oxygenated species at higher electrode potentials. Also the XANES region indicates a slight tendency of reduction in the Au 5*d* band occupancy due the presence of silver. Electrochemical testing showed that nanoparticles synthesized by glycerol as reducing chemical method presents interesting catalytic activity. Ligand effect has been found to play a major role for the glycerol electro-oxidation. This may be ascribed to the electron withdrawing of the Ag atoms present in the gold surface that reduces the Au density of states close to the Fermi level and may induce changes in the adsorption strength of adsorbates on the Au surface.

Acknowledgments

The authors thank Fundação de Amparo à Pesquisa do Estado de São Paulo (FAPESP) (particularly, process n. 2012/10856-7) and Conselho Nacional de

Desenvolvimento Científico e Tecnológico (CNPq) for financial support and Brazilian National Laboratory of Synchrotron Light (LNLS) for the XAS analyses.

References

[1]Schmid, G. *Clusters & Colloids: From Theory to Application*; VCH: Weinheim 1994

[2]Kamat, P. V.; Meisel, D. Studies in Surface Science and Catalysis; *Semiconductor Nanoclusters - Physical*, *Chemical*, *and Catalytic Aspects*; Elsevier: Amsterdam, **1997**, 103.

[3]Ditlbacher, H. Lamprecht B, Leitner A, Aussenegg FR., Spectrally coded optical data storage by metal nanoparticles. Opt Lett. **2000**, 25(8), 563-565.

[4]Kneipp, K. Haka, A. S. Kneipp, H. Badizadegan, K. Yoshizawa, N. Boone, C. Shafer-Peltier, K. E. Motz, J. T. Dasari, R. R. Feld, M. S. Surface-Enhanced Raman Spectroscopy in Single Living Cells Using Gold Nanoparticles. Appl. Spectroscopy. **2002**, 56-2,150-154.

[5]Herricks, T. Chen, J. Xia, Y. Polyol synthesis of platinum nanoparticles: Control of morphology with sodium nitrate. Nano Lett. **2004**, 12, 2367-2371.

[6]Raghuveer, M. S. Agrawal, S. Bishop, N. Ramanath, G. Microwave-assisted single-step functionalization and in situ derivation of carbon nanotubes with gold nanoparticles. Chem. Mater. **2006**, 18, 1390-1393.

[7]Lu, C. Rice, C Masel, R. I. Babu, P. K. Waszczuk, Kim, H. S. Oldfield, E. Wieckowski, A. UHV, Electrochemical NMR, and Electrochemical Studies of Platinum/Ruthenium Fuel Cell Catalysts. J. Phys. Chem. *B*. **2002**, 106 (37), 9581–9589.

[8]Liu, P. Logadottir, A. Norskov, J. K. Electrochim. Acta. **2003,** 48, 3731.

[9]Gasparotto, L. H. S. Garcia, A. C. Gomes, J. F. Tremiliosi-Filho, G. Electrocatalytic performance of environmentally friendly synthesized gold nanoparticles towards the borohydride electro-oxidation reaction. J. Power Sources. **2012**, 218, 73-78.

[10]Garcia, A. C. Gasparotto, L. H. S. Gomes, J. F. Tremiliosi-Filho, G. Straightforward synthesis ofof carbon-supported Ag nanoparticles and their application for the oxygen reduction reaction. Electrocatalysis. 2012, 3, 1-6.

[11]West, A.R. In: Solid state chemistry and its applications (Wiley, New York, 1984), 742.

[12]Camara, G. A. Giz, M. J. Paganin, V. A. Ticianelli, E. A. Correlation of electrochemical and physical properties of PtRu alloy electrocatalysts for PEM fuel cells. J. Electroanal. Chem. **2002**, 537, 21-29.

[13]Daniel, M. C. & Astruc, D. Gold nanoparticles: Assembly, supramolecular chemistry, quantum-size-related properties, and applications toward biology, catalysis, and nanotechnology. Chemical Reviews, 2004, 104, 293-346.

[14]Moskovits, M. Srnova-Sloufova, I. & Vlckova, B. Bimetallic Ag-Au nanoparticles: Extracting meaningful optical constants from the surface-plasmon extinction spectrum. J. Chem. Phys. **2002**, 116, 10435-10446.

[15]Mulvaney, P. Surface Plasmon Spectroscopy of Nanosized Metal Particles. Langmuir. **1996**, 12, 788-800.

[16]Link, S. Wang, Z. L. & El-Sayed, M. A. Alloy Formation of Gold−Silver Nanoparticles and the Dependence of the Plasmon Absorption on Their Composition. J. Phys. Chem. B, **1999**, 103, 3529-3533.

[17]Polavarapu, L and Liz-Marzán, L. M. Growth and galvanic replacement of silver nanocubes in organic media. *Nanoscale*, **2013**, 5, 4355.

[18]Sun,Y and Xia, Y. Mechanistic Study on the replacement reaction between silver nanostructures and chloroauric acid in aqueous medium. *J. Am. Chem. Soc.*, **2004**, *126* (12), 3892–3901.

[19]Sun, Y. and Wang, Y. Monitoring of galvanic replacement reaction between silver nanowires and HAuCl4 by in situ transmission X-ray microscopy. *Nano Lett*. **2011**, 11, 4386–4392.

[20]Rodríguez-González ,B., Burrows, A., Watanabe, M., Kielyb, C. J., Liz-Marzán, L. M. Multishell bimetallic AuAg nanoparticles: synthesis, structure and optical properties. J. Mater. Chem., **2005**, 15, 1755–1759.

[21]Joint Committee on Powder Diffraction Standards (1980) JCPDS, Pennsylvania

[22]Déonzier, T. Morfin, F. Lomello, M. Rousset. J. Catalysis on nanoporous gold–silver systems: Synergistic effects toward oxidation reactions and influence of the surface composition. J. Catalysis. **2014**, 311, 221–229.

[23]Russell, A. E. Maniguet, S. Mathew, R. J. Mark, J. Y. Roberts, M. A. Thompsett, D. In situ X-ray absorption spectroscopy and X-ray diffraction of fuel cell electrocatalysts. J. Power Sources. **2001**, 96, 226-232.

[24]Christoffersen, E. Liu, P. Ruban, A. Skriver, H. L. Norkov, J. K. Anode materials for low-temperature fuel cells: A density funcition theory study. J. Catalysis, **2001**, 199, 123-131.

[25]Mukerjee, S. Srinivasan, S. Soriaga, M. P. McBreen, J. Role os structural and electronic properties of Pt and Pt alloys on electrocatalysis of oxygen reduction – An in situ XANES and EXAFS investigation. J. Electrochem. Soc**. 1995**, 142, 1409-1422.

[26]Savinova, E.R.; Kraft, P.; Pettinger, B.; Doblhofer, K. In situ Raman spectroscopy studies of the interface between silver (111) electrodes and alkaline NaF electrolytes. J. Electroanal. Chem. **1997**, 430, 47-56.

[23] Orozco, G. Perez, M. C. Rincon, A. Gutierrez, C. Electrooxidation of methanol on silver in alkaline medium. J. Electroanal. Chem. **2000**, 495, 71-78.

Table 1: Mean crystallite size calculated from Scherrer equation, particle size from TEM analysis and lattice parameter.

Catalyst	Crystallite size / nm	Particle size / nm	Lattice Parameter / A
Au/C	17	9	4.072
Ag/C	19	16	4.084
$Au_{50}Ag_{50}$/C	14	17	4.082

Table 2 – Summary of the structural parameters obtained from the EXAFS data fitting for both Au and AuAg-NPs/C. For comparison is also shown the parameters obtained for gold foil. The parenthesis number stands for the standard deviation in the parameter determination, where 0.001(1) is equal to 0.001±0.001.

Au-foil (ex-situ)					
Au-Au	N	12.0(6)			
shell	R / Å	2.863(3)			
	σ^2 / Å^2	0.0085(5)			
Au/C					
		OH - sol		OH – sol + glycerol	
		0.5 V	0.95 V	0.5 V	0.95 V
Au-Au	N	12.2(8)	12(1)	11(1)	12(1)
shell	R / Å	2.853(5)	2.860(7)	2.863(8)	2.866(7)
	σ^2 / Å^2	0.009(1)	0.009(1)	0.008(1)	0.009(1)
AuAg/C					
		OH - sol		OH – sol + glycerol	
		0.5 V	0.95 V	0.5 V	0.90 V
Au-Au	N	9(4)	12(5)	9(2)	15(2)
shell	R / Å	2.85(2)	2.87(3)	2.83(2)	2.87(1)
	σ^2 / Å^2	0.008(5)	0.011(6)	0.005(3)	0.016(2)
Au-Ag	N	1(1)	0.3(8)	0.7(5)	0.8(5)
shell	R / Å	2.79(5)	2.84(5)	2.74(3)	2.92(1)
	σ^2 / Å^2	0.001(8)	0.01(1)	0.004(4)	0.002(4)

FIGURE CAPTION

Fig. 1: A) UV-Vis spectra of the colloidal Au, Ag and AuAg NPs. Condition of synthesis of the monometallic NPs: 0.1 mmol L^{-1} Au^{3+} or 0.1 mmol L^{-1} Ag^{+1}, 0.5 mol L^{-1} glycerol, 0.01 mol L^{-1} NaOH and 10 g L^{-1} PVP. Condition of synthesis of the AuAg bimetallic NPs: 0.05 mmol L^{-1} Au^{3+}, 0.05 mmol L^{-1} Ag^{+}, 0.5 mol L^{-1} glycerol, 0.01 mol L^{-1} NaOH and 10 g L^{-1} PVP and B) TEM images of the colloidal Au, Ag and AuAg NPs.

Fig. 2: A) UV-Vis spectra of the colloidal silver nanoparticles with subsequent addition of $HAuCl_4$. B) UV-Vis spectra of the colloidal gold nanoparticles with subsequent addition of $AgNO_3$. Final concentrations of the added salts are shown in the figures. Condition of synthesis of the monometallic NPs: 0.20 mmol L^{-1} Au^{3+} or 0.20 mmol L^{-1} Ag^{+1}, 0.1 mol L^{-1} glycerol, 0.01 mol L^{-1} NaOH and 10 g L^{-1} PVP.

Fig. 3: A) X-ray diffraction (XRD) pattern of the Au/C, Ag/C and AuAg/C and B) TEM images of the Au, Ag and AuAg catalysts dispersed onto Vulcan carbon.

Fig. 4: (A) EXAFS signal at Au L_3 edge. (B) Fourier transformed of the oscillations.

Fig. 5: (A) UV-Vis spectra of the colloidal AgNPs from AgCl Condition of synthesis: 0.1 mol L^{-1} KCl with 0.1 mol L^{-1} $AgNO_3$ and (B) Kinetics of formation of AuNPs and AgNPs. In both cases the concentration of metallic ions was 0.1 mmol L^{-1}.

Fig. 6: XANES spectra for Au/C and AuAg/C electrocatalysts at 0.5 and 0.95V.

Fig. 7: Cyclic voltammograms for Au/C, Ag/C and AuAg/C electrocatalysts obtained at 50 mV s^{-1} in NaOH 0.1 M and NaOH 0.1 M + glycerol 0.1 M. All experiments were conducted at room temperature. (geometric area of the electrode = 0.196 cm^2)

Figure 1

A

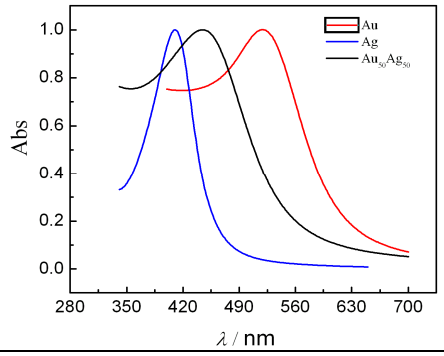

B

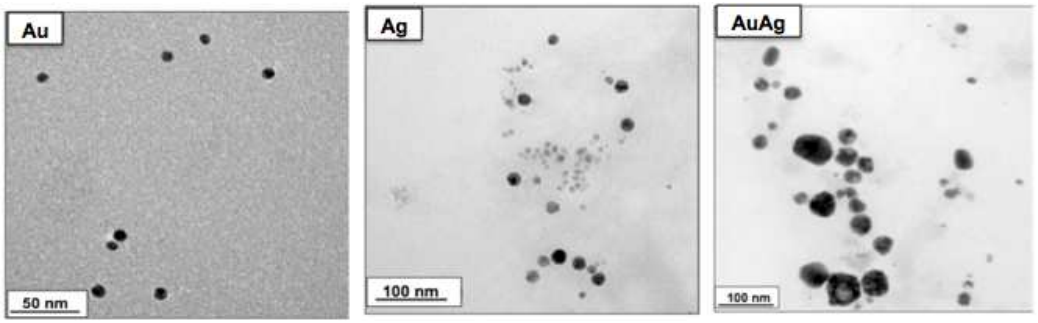

Figure 2A

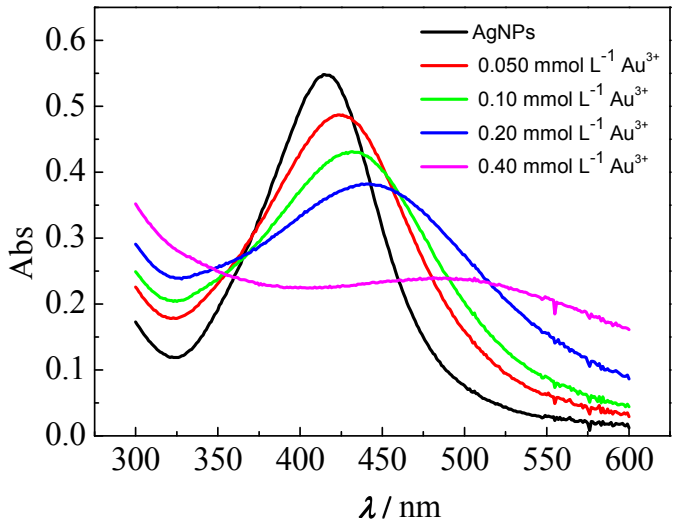

Figure 2B

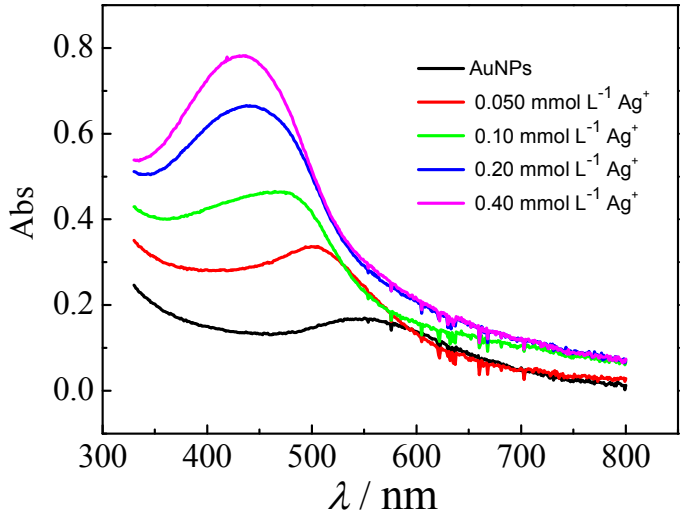

Figure 3

A

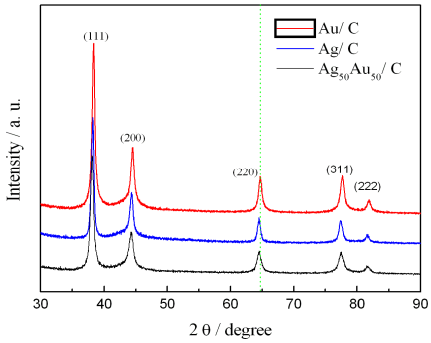

B

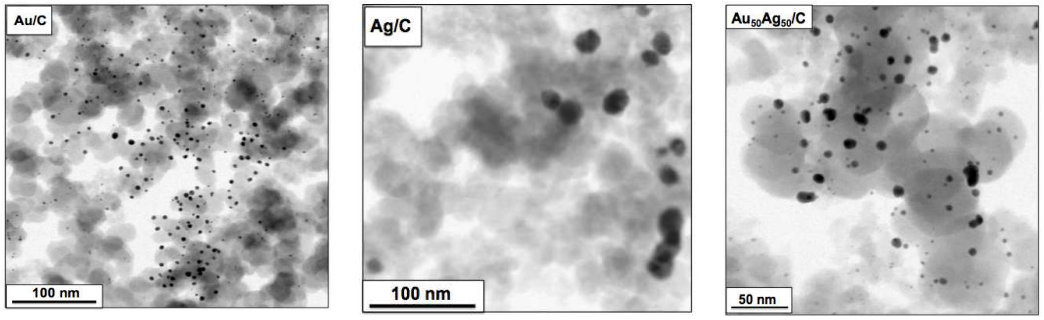

Figure 4

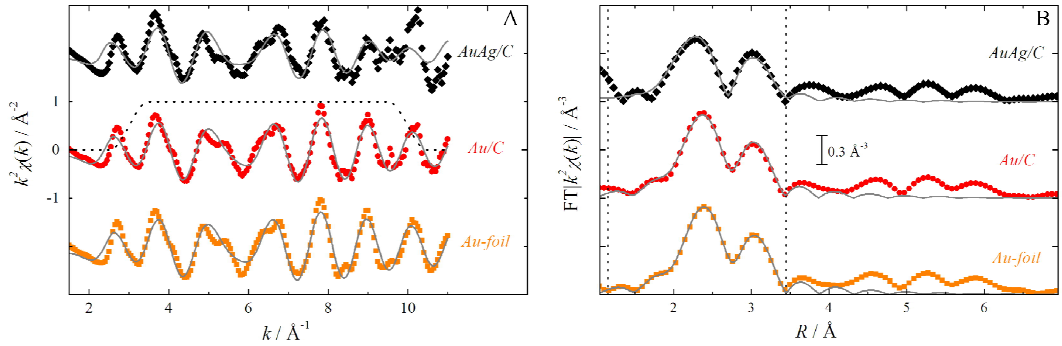

Figure 5

(A)

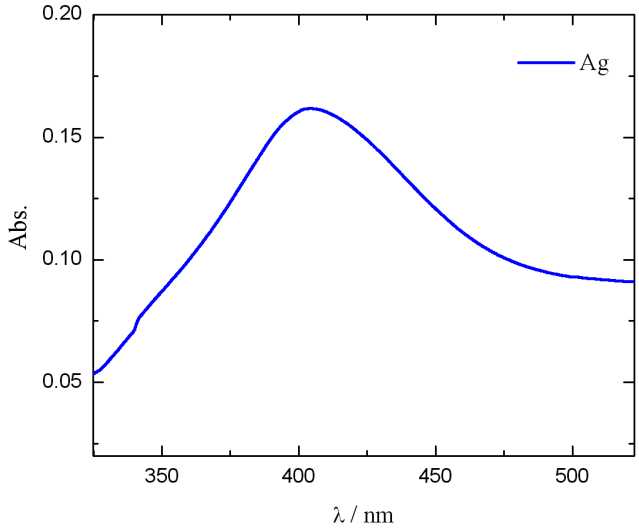

(B)

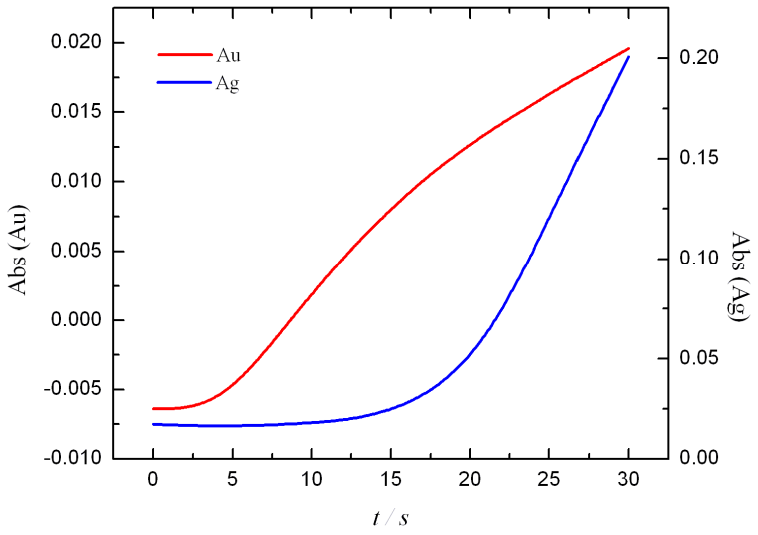

Figure 6

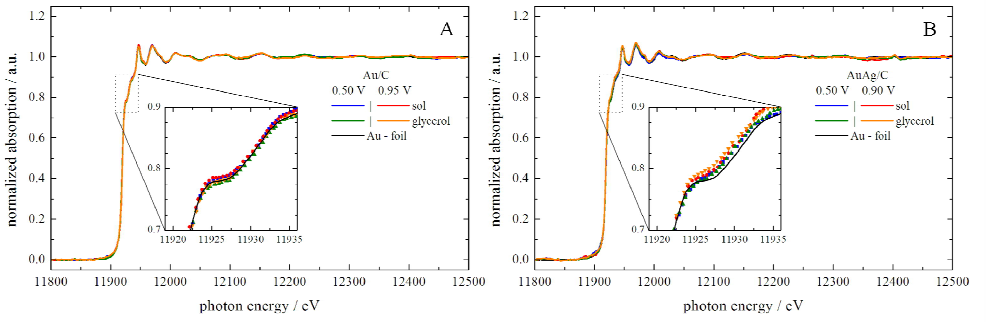

Figure 7